HAL
open science

Effects of multiply charged ions on microturbulence-driven electron transport in partially magnetized plasmas

P. Kumar, S. Tsikata, K. Hara

To cite this version:

P. Kumar, S. Tsikata, K. Hara. Effects of multiply charged ions on microturbulence-driven electron transport in partially magnetized plasmas. Journal of Applied Physics, 2021, 130 (17), pp.173307. 10.1063/5.0067305 . hal-03433522

HAL Id: hal-03433522

https://hal.science/hal-03433522v1

Submitted on 26 Nov 2022

HAL is a multi-disciplinary open access archive for the deposit and dissemination of scientific research documents, whether they are published or not. The documents may come from teaching and research institutions in France or abroad, or from public or private research centers.

L'archive ouverte pluridisciplinaire **HAL**, est destinée au dépôt et à la diffusion de documents scientifiques de niveau recherche, publiés ou non, émanant des établissements d'enseignement et de recherche français ou étrangers, des laboratoires publics ou privés.

ACCEPTED MANUSCRIPT

Journal of Applied Physics

This is the author's peer reviewed, accepted manuscript. However, the online version of record will be different from this version once it has been copyedited and typeset.
PLEASE CITE THIS ARTICLE AS DOI: 10.1063/5.0067305

Effects of multiply charged ions on microturbulence-driven electron transport in partially magnetized plasmas

P. Kumar,[1] S. Tsikata,[2] and K. Hara[1]

[1)] *Department of Aeronautics and Astronautics, Stanford University, California 94305, USA*

[2)] *ICARE UPR 3021, Centre National de la Recherche Scientifique (CNRS), 45071 Orléans, France*

(*Electronic mail: kenhara@stanford.edu)

(*Electronic mail: prkumar@stanford.edu)

(Dated: 4 October 2021)

Nonlinear interaction between kinetic instabilities in partially magnetized plasmas in the presence of multiply-charged ion streams is investigated using kinetic simulations. It was observed by Hara and Tsikata [Phys. Rev. E **102**, 023202 (2020)] that the axial ion-ion two-stream instability (IITSI) due to singly and doubly charged ion streams, coupled with the azimuthal electron cyclotron drift instability (ECDI), enhances cross-field electron transport. In the present study, it is observed that the addition of triply charged ions (as a third ion species) contributes to damping of the excited modes, leading to a reduction in the cross-field electron transport. The net instability-driven electron transport is shown to be a function not only of the azimuthal modes, such as the ECDI, but of the multiple ion species that dictate the development of additional plasma waves. It is found that trapping of the higher ion charge states within the plasma waves results in a broadening of the ion velocity distribution functions.

I. INTRODUCTION

Cross-field electron transport across magnetic field lines plays an important role in fusion, astrophysical, and $\mathbf{E}\times\mathbf{B}$ discharge plasmas[1,2]. While cross-field discharges have been widely studied theoretically[3–6], experimentally[7–10], and numerically[11–14], turbulent transport of electrons across the magnetic field is still not well understood. Experimentally measured electron transport has been shown to be significantly higher than that predicted from classical collisional transport processes.

Over the last few decades, a number of different models, using fluid[11,15,16], kinetic[17–20], and hybrid approaches[21–23], have been proposed to explain these phenomena. Fully kinetic particle-in-cell (PIC) models have been recently used to investigate the role of plasma turbulence induced by kinetic instabilities on the cross-field transport of electrons. While electron diffusion across the magnetic field lines can be caused by fluctuations in the electric field in the $\mathbf{E}\times\mathbf{B}$ direction alone, microturbulence may be driven by nonlinear coupling between different linear instabilities[24–26] and can influence the cross-field electron mobility[14,27]. In developing reduced-order models for electron transport, accounting for the effects of such mode coupling is necessary.

The existence of a variety of charge states within such plasmas has additional wide-ranging implications. Depending on the discharge characteristics, such as the operating power, triply and even quadruply charged ions can be generated in addition to the singly and doubly charged ions in HETs[28]. The generation of higher charge states is also a known feature of other $\mathbf{E}\times\mathbf{B}$ devices such as planar magnetrons[29] operating in high-current pulsed regimes. Ions of different species also result in complex kinetic phenomenon, such as the mixture of ion species near the plasma sheaths[30] and light ions potentially stabilizing plasma turbulence[31].

Previous work by Hara and Tsikata in Ref. 32 investigated the coupling between the electron cyclotron drift instability (ECDI) and ion-ion two-stream instability (IITSI) in Hall effect thrusters (HETs) due to the mixture of singly and doubly charged ion streams using kinetic theory and simulations. The relative velocity between singly and doubly charged ion streams causes the excitation of the IITSI, first identified and studied in coherent Thomson scattering measurements[25]. In addition, it was shown in Ref. 32 that cross-field electron transport is enhanced due to the multidimensional plasma waves initiated by the coupling between ECDI in the azimuthal direction (in the direction of the $\mathbf{E}\times\mathbf{B}$ drift) and IITSI in the axial direction (in the direction of the applied $\mathbf{E}$ field).

In the present paper, we now analyze a more complex, but physical, case involving three ion populations using the axial-azimuthal PIC simulation. We consider the case in which a large-amplitude IITSI due to singly and doubly charged xenon ions is present while the ECDI is initiated in the cross-field direction. A third species of triply charged xenon ions is then introduced in the simulations and their effects on the multidimensional plasma wave and cross-field plasma transport are investigated by varying the triply charged ion fraction. Charged species streaming with different velocities nonlinearly interact with the plasma wave, leading to particle trapping that influences the nonlinear saturation of these instabilities. The trapping mechanisms for the three species considered in the simulation and their impact on the corresponding velocity distribution function (VDF) is also analyzed.

This paper is organized as follows. The simulation method and physical and numerical parameters are described in Section II. Section III A discusses the coupling of ECDI and IITSI. In Section III B, the wave damping due to triply charged ions is analyzed. The effect of the wave damping on cross-field electron transport is discussed in Section III C. Finally, broadening of ion VDFs and nonlinear trapping of ion species

ACCEPTED MANUSCRIPT
Journal of Applied Physics
AIP Publishing
This is the author's peer reviewed, accepted manuscript. However, the online version of record will be different from this version once it has been copyedited and typeset.
PLEASE CITE THIS ARTICLE AS DOI: 10.1063/5.0067305

is presented in Section III D.

II. SIMULATION METHOD AND PARAMETERS

The 2D axial-azimuthal Particle-in-Cell (PIC) model originally proposed by Boeuf and Garrigues[14] and later utilized by Charoy et al.[13] and Hara et al.[32] is adapted and further extended to incorporate a triply charged ion species in the simulations.

A 2D Cartesian domain in the axial (x) and azimuthal (y) plane with axial length $L_x = 2.5$ cm and azimuthal length $L_x = 1.28$ cm is discretized uniformly using 500 and 256 cells, respectively. At the beginning of the simulations, electrons and ions are loaded uniformly with a density of 5.0×10^{16} m^{-3} and a Maxwellian velocity distribution with electron temperature, $T_e = 10$ eV, and ion temperature, $T_i = 0.5$ eV. While the collisions are neglected in this setup, ionization events are modeled using an ionization rate function, $S_i(x)$, assumed constant in time, leading to a constant ion current density in steady state[14]. The steady-state continuity equation for the ions can be written as,

$$\nabla \cdot (\mathbf{j}_{i1} + \mathbf{j}_{i2} + \mathbf{j}_{i3}) = e(S_{i1} + 2S_{i2} + 3S_{i3}),$$

where $\mathbf{j}_{ik}$ is the ion current density, e is the elementary charge, and S_{ik} is the ionization rate for $k = 1,2,3$ corresponding to singly, doubly, and triply charged ion species, respectively. We define α_d and α_t to be the fraction of doubly and triply charged ion current densities with respect to the total ion current density, such that the individual source terms are assigned as $S_{i1} = (1-\alpha_d-\alpha_t)S_i(x)$, $S_{i2} = \alpha_d S_i(x)/2$, and $S_{i3} = \alpha_t S_i(x)/3$. Here, the total ionization rate $S_i(x)$ is defined as

$$S_i(x) = S_0 \cos\left(\pi \frac{x - x_M}{x_2 - x_1}\right),$$

where $x_1 = 0.25$ cm, $x_2 = 1.0$ cm, $x_M = (x_1 + x_2)/2$, and S_0 is adjusted to impose $j_M = 400$ A/m^2 to be the total ion current density.

The radial magnetic field is applied in the axial (x) direction, given by $B(x) = B_{\max} + B_0 \xi(x)$, where

$$\xi(x) = 1 - \exp\left[1 - \left(\frac{x - x_L}{2\sigma_b}\right)^2\right]$$

and $B_0 = (B_a - B_{\max})/\xi(0)$ if $x < x_L$ and $B_0 = (B_c - B_{\max})/\xi(x_L)$ if $x \geq x_L$. Here, $x_L = 0.75$ cm, $\sigma_b = 0.625$ cm, $B_{\max} = 100$ G, $B_a = 60$ G, and $B_c = 10$ G. Neutral atom dynamics and transport is not taken into account. Periodic boundary conditions are used in the azimuthal direction. The anode plane, located at the left axial boundary is kept at a fixed potential of 200 V. At the cathode plane, i.e., $x = 2.4$ cm, the azimuthally averaged potential is set to be zero[14], and the electrons are injected from a random position in the azimuthal direction maintaining current conservation, i.e., $\Gamma_{ec} = \Gamma_{ea} - \Gamma_{i1a} - 2\Gamma_{i2a} - 3\Gamma_{i3a}$, where Γ_{ec} is the number of electrons re-injected from the cathode plane, and $\Gamma_{ea}, \Gamma_{i1a}, \Gamma_{i2a}$, and Γ_{i3a} are the number of electrons, singly charged ions, doubly charged ions, and triply charged ions absorbed at the anode plane, respectively.

An explicit PIC code, developed within the Plasma Dynamics Modeling Laboratory at Stanford University and benchmarked against several different codes in the community, is utilized for the simulations presented in this paper[13,32]. The code is written in C++ and utilizes Message Passing Interface (MPI) for particle decomposition. The Poisson equation is solved using the scalable linear solver library, HYPRE. Simulations are performed with a grid size of 50 μm in both directions and the number of particles per cell reaches approximately 250 in the steady state. Numerical convergence studies have shown that these parameters are sufficient for resolving the physics processes of interest in this paper.

III. RESULTS AND DISCUSSION

The effect of increasing the fraction of triply charged ion species (α_t) in addition to singly and doubly charged ions is studied. The results presented in the paper use a condition in which the doubly charged ion fraction is fixed $(\alpha_d = 20\%)$ such that a large-amplitude IITSI coexists with ECDI[32] and the triply charged ion fraction is varied $\alpha_t = 0 - 10\%$. The plasma wave behavior reaches a steady state around $10 - 15$ μs and the simulations are run up to 30 μs to ensure that the plasma wave characteristics do not diverge.

A. Coupling between ECDI and IITSI

Figure 1 shows the instantaneous azimuthal (E_y) and axial (E_x) electric field due to coupling between ECDI and IITSI for $\alpha_t = 0$ in the top row and 10% in the bottom row, respectively, in steady state. The results without the triply charged ions (top row) are identical to the cases presented in Ref. 32. Here, the addition of triply charged ions (bottom row) similarly shows the coexistence of ECDI (modulation along y) and IITSI (modulation along x). The azimuthal plasma wave observed in the simulation exhibits wavelength corresponding to the resonance at $k_y \lambda_D \approx 0.9$, where the ECDI growth rate is maximum. The dominant wavelength of axial fluctuation is on the scale of 1 mm driven by the IITSI. As discussed in Ref. 32, the simulation results show that the ECDI is primarily driven in the region where $E \times B$ drift is largest ($x \in [0.5$ cm,1 cm] in this simulation) and the IITSI is driven in the region where the velocity difference between Xe^+ and Xe^{2+} increases ($x \geq 1$ cm in this simulation).

B. Wave damping due to addition of triply charged ions

As the fraction of triply charged xenon ions (Xe^{3+}) is increased, damping of the the plasma wave amplitude can be seen. To further quantitatively investigate such damping in the presence of triply charged ions, we perform fast Fourier transform (FFT) analysis of the two-dimensional electric field

ACCEPTED MANUSCRIPT
Journal of Applied Physics
AIP Publishing
This is the author's peer reviewed, accepted manuscript. However, the online version of record will be different from this version once it has been copyedited and typeset.
PLEASE CITE THIS ARTICLE AS DOI: 10.1063/5.0067305

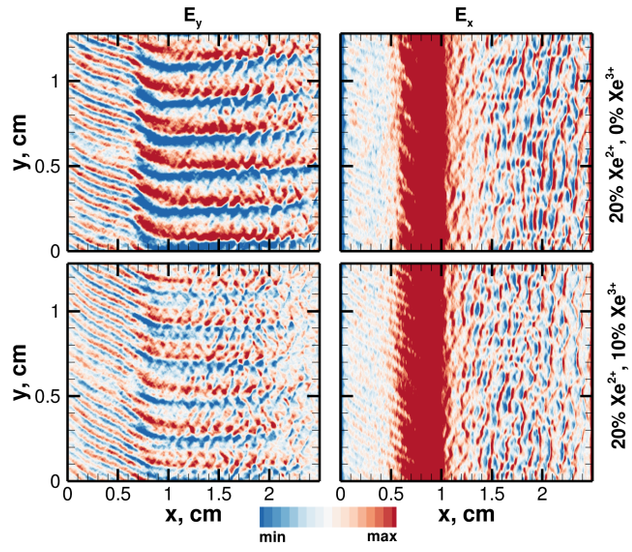

FIG. 1: Effect of increasing triply charged ion concentration on instantaneous azimuthal (E_y) and axial (E_x) electric field due to coupling between ECDI and IITSI. Top row: $\alpha_d = 20\%$ and $\alpha_t = 0$; bottom row: $\alpha_d = 20\%$ and $\alpha_t = 10\%$. Results are shown for $t = 18$ μs, i.e., after the steady state is reached. The colorbar is saturated for better visualization of axial fluctuations in the downstream region, where min and max on the color scale correspond to -2.0×10^4 V/m and 2.0×10^4 V/m, respectively.

components in the plume, within $x \in [1.4$ cm, 2.4 cm$]$ and $t = [15\ \mu$s, $20\ \mu$s$]$.

Amplitudes of the FFT of azimuthal field (E_y) and axial field (E_x) are shown in the (k_x, k_y) plane for the 0% Xe^{3+} case in Figs. 2(a1) and (b1), respectively. The peaks at $k_x = 0$ in Fig. 2(a1) correspond to the resonance modes of the ECDI. Additionally, signatures of axial fluctuation of E_y are evident in the bright spots at $k_x \neq 0$, suggesting that the axial oscillations of E_y are correlated with the axial oscillations of E_x due to the IITSI, as shown in Fig. 2(b1). However, the ECDI resonances in the E_y spectra are not found in the E_x spectra, indicating that the axial plasma waves (E_x) are not influenced by the ECDI. This is because the ions are accelerated to velocities that can initiate the IITSI *downstream* of the region in which the ECDI occurs at $k_x = 0$ due to the large $\mathbf{E} \times \mathbf{B}$ drift.

Figures 2(a2) and (b2) show the results when the fraction of triply charged ions is increased from 0% to 10%. While the FFT results show a structure similar to the case without triply charged ions, there is a slight change in the amplitude of the electric field fluctuations. Figure 2(a3) shows the FFT of E_y as a function of k_y, i.e., the results in Figs. 2(a1) and (a2) integrated in k_x. It can be seen that the amplitude of the azimuthal field E_y in the plume decreases approximately 30%, when 10% triply charged xenon ions are added ($\alpha_t = 0.1$). This is noteworthy since the electric field investigated here is within the plume. As shown later in Fig. 3(d), the time-averaged, azimuthally-averaged axial electric field is not modified due to the presence of triply charged ions, meaning that the maximum $\mathbf{E} \times \mathbf{B}$ drift around $x \in [0.5$ cm, 1 cm$]$ remains unchanged. Hence, the azimuthal wave initiated by the $\mathbf{E} \times \mathbf{B}$ drift would not be locally affected, if there is no influence from other regions of the plasma flow. Additionally, using the 2D linear dispersion theory in Ref. 32, the ECDI growth rate was found to be unaffected by the presence of multiply charged ions. The decrease in the E_y amplitude shown in Fig. 2(a3) is thus unexpected, as the results indicate that the axial IITSI in the presence of of Xe^{3+} affects the azimuthal wave (the E_y fluctuation) that is primarily driven by ECDI in the region where $\mathbf{E} \times \mathbf{B}$ drift is largest. The effects of mode damping in the presence of light and heavy ion species have been shown in different contexts, as was mentioned in the introduction[31,33]. It is interesting to note that in the present case, significant mode damping effects occur due to the presence of multiple ion species of the same mass but with different velocities. With differing charge states, these species reshape the distribution of energy in the fluctuations via their response to the applied accelerating field.

Finally, Fig. 3(b3) shows that the amplitude of the axial field FFT$|(E_x)|$, integrated along k_y and plotted against k_x, decreases nearly 8% when triply charged ions are present. Since the linear dispersion theory indicates that the growth rate of the IITSI is unaffected by the presence of triply charged ions, the observed reduction of the plasma wave amplitude is due to the nonlinear dynamics between multiply charged ion streams. As will be shown later, multiply charged ions have a different bounce frequency due to particle trapping within the plasma wave. It is likely that such nonlinear phenomena lead to the waves having more temporal and spatial modes, leading to the damping of the plasma wave amplitude.

C. Effect of multiply charged ions on cross-field electron transport

Electron transport in the cross-field direction can be characterized by the axial electron bulk velocity[12,34]:

$$u_{e,\perp} = -\mu_\perp \left(E_\perp + \frac{1}{en_e} \nabla_\perp p_e \right), \tag{1}$$

considering the drift-diffusion approximation, i.e., in steady state and when the inertia terms are negligible. Here, $u_{e,\perp}$ is the cross-field electron bulk velocity, $\mu_\perp$ is the cross-field mobility, $E_\perp = E_x$ is the axial electric field, and p_e is the electron pressure. Note that when collisional processes are dominant, the cross-field mobility can be derived as $\mu_\perp = \mu_0(1+\Omega^2)^{-1}$, where $\mu_0 = e/(m_e \nu_m)$ is the unmagnetized electron mobility, m_e is the electron mass, ν_m is the electron momentum transfer collision frequency, $\Omega = \omega_B/\nu_m$ is the Hall parameter, and $\omega_B = eB/m_e$ is the electron gyrofrequency.

Figure 3 shows the plasma properties averaged in the y direction and over a 5 μs period in the steady state. The changes in the Xe^+ density as α_t is varied while keeping $\alpha_d = 20\%$ can be seen in Fig. 3(a). There is no notable change in the doubly charged ion density as $\alpha_d = 20$ % is used for all cases, as shown in Fig. 3(b), and Fig. 3(c) shows that the triply charged

ACCEPTED MANUSCRIPT
Journal of Applied Physics
AIP Publishing
This is the author's peer reviewed, accepted manuscript. However, the online version of record will be different from this version once it has been copyedited and typeset.
PLEASE CITE THIS ARTICLE AS DOI: 10.1063/5.0067305

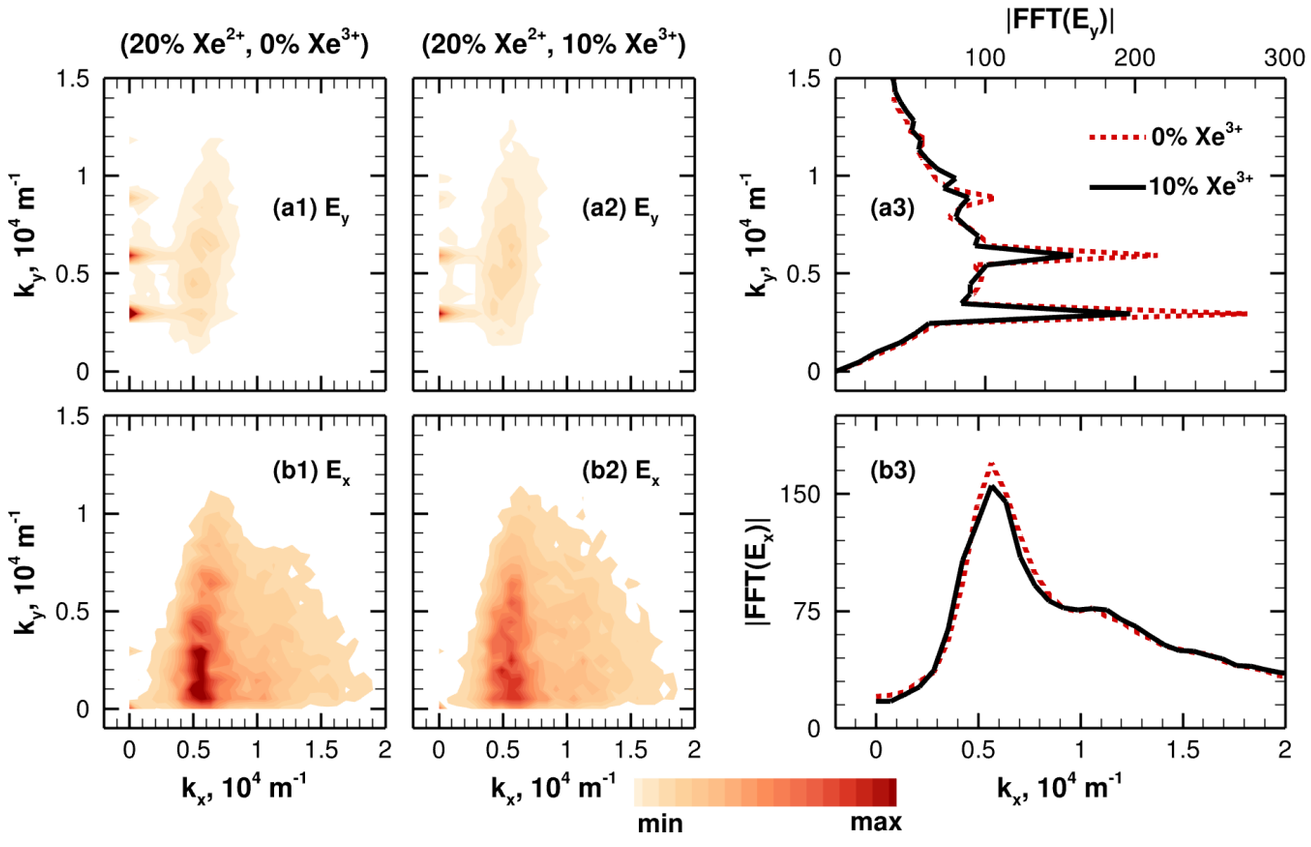

FIG. 2: Damping of ECDI and IITSI in the presence of singly, doubly, and triply charged ions. $\alpha_d = 20\%$ is fixed while α_t is varied. Color plots show 2D FFT of time-averaged azimuthal (E_y) and axial (E_x) fields in steady state in the (k_x, k_y) plane: (a1) FFT(E_y) with $\alpha_t = 0\%$, (a2) FFT(E_y) with $\alpha_t = 10\%$. (b1) FFT(E_x) with $\alpha_t = 0\%$, and (b2) FFT(E_x) with $\alpha_t = 10\%$. Min and max values on the colorbar correspond to 100 and 1500 for (a1) and (a2), respectively, and 100 and 4000 for (b1) and (b2), respectively. The line plots (a3) and (b3) are obtained from the 2D data by integrating with respect to k_x and k_y respectively: (a3) shows the variation in the azimuthal electric field amplitude as a function of k_y; (b3) shows the variation of the axial electric field amplitude as a function of k_x.

ion density increases proportional to α_t. While the axial electric field, shown in Fig. 3(d), is slightly damped, the overall structure is not modified and the difference at the peak is within 4% with increasing fraction of triply charged ions. Since the contribution from the pressure gradient, i.e., diffusion flux, is smaller than the drift flux due to the electric field[35,36] within the acceleration and plume regions, the results shown in Fig. 3 indicate that the cross-field electron mobility is proportional to $|u_{e,\perp}|$.

Figure 4 shows the time-averaged, azimuthally-averaged axial electron velocity, $u_{e,\perp}$, for different triply charged ion fractions. The electron bulk velocities shown here are obtained by averaging in the y direction and over a 5 μs period in the steady state between 15 and 20 μs. Note that the values are negative as the electrons travel toward the anode (to the left of the computational domain). The baseline case, $\alpha_d = 20\%$ and $\alpha_t = 0\%$, is identical to the results in Ref. 32. As the fraction of triply charged ions is increased by varying α_t to 5% and 10%, a consistent reduction in the absolute value of axial electron velocity is observed. While the electron bulk velocity in the upstream, e.g., $x \in [0\text{ cm}, 0.3\text{ cm}]$, is not affected by the triply charged ions, the decrease in the electron bulk speed is approximately 20% when $\alpha_t = 10\%$ from the case when $\alpha_t = 0$.

Since the bulk plasma properties remain virtually unchanged to this incremental change in the triply charged ion fraction, as discussed in Fig. 3, it can be concluded that the decreased axial electron bulk velocity is caused by the reduction in the anomalous electron mobility. It is to be noted that the net ion current density in the system is constant, as discussed in Section II. While it was shown in Ref. 32 that the generation of IITSI due to Xe^{2+} and Xe^{+} in addition to the ECDI enhances the cross-field electron mobility, Fig. 4 shows that the addition of Xe^{3+} results in a slight reduction of the enhanced cross-field electron mobility. It was discussed in Ref. 32 that the cross-field electron flux density in the presence of plasma turbulence can be written as, $\Gamma_{e,x} = \langle n'_e E'_y \rangle / B_z$, where n'_e and E'_y are the fluctuations of the electron density and electric field, respectively, and the bracket denotes temporal and spatial average. The reduced electron transport across magnetic field is

ACCEPTED MANUSCRIPT
Journal of Applied Physics
AIP Publishing
This is the author's peer reviewed, accepted manuscript. However, the online version of record will be different from this version once it has been copyedited and typeset.
PLEASE CITE THIS ARTICLE AS DOI: 10.1063/5.0067305

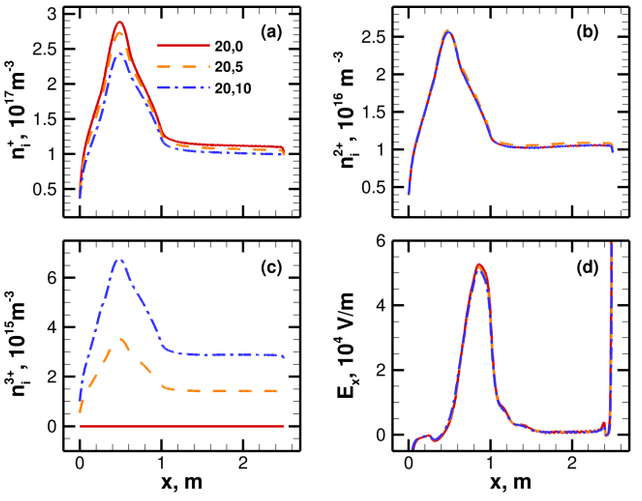

FIG. 3: Spatially and temporally averaged plasma properties. All quantities are averaged in y direction and over 5 μs period in steady state. (a) Xe^+ density, (b) Xe^{2+} density, (c) Xe^{3+} density, and (d) axial electric field. All the physical and numerical parameters are fixed while $\alpha_d = 20$ % and α_t is varied. Three cases corresponding to $\alpha_t = 0, 5$ and 10% are shown.

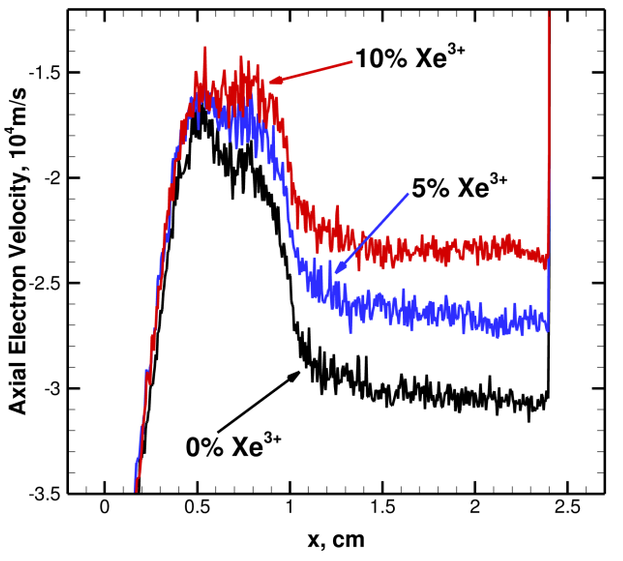

FIG. 4: Cross-field electron transport is reduced when increasing triply charged ion species fraction. Plasma properties are averaged in y direction and over 5 μs from $t = 15\ \mu\text{s} - 20\ \mu\text{s}$. For all cases, $\alpha_d = 20\%$ is used and the results for $\alpha_t = 0$, 5%, and 10% are shown.

therefore likely to be attributed to the dampened electric field amplitudes, shown in Fig. 2. The results indicate that the amplitude of the microturbulence developed due to the coupling between ECDI and IITSI affects the cross-field electron transport in the presence of ion species streaming with different velocities.

D. Nonlinear ion wave trapping

The charged particles can be trapped within the axial plasma wave initiated by the IITSI and the azimuthal plasma wave initiated by the ECDI, resulting in a non-Maxwellian ion velocity distribution (IVDF). Here, the axial and azimuthal IVDFs of Xe^+, Xe^{2+}, and Xe^{3+} are presented.

1. *Axial IVDF*

The bulk velocity of ions that accelerate across a constant discharge voltage V_d can be calculated as

$$U_x^{Z+} = \left(\frac{2ZeV_d}{m_i}\right)^{1/2}, \tag{2}$$

where $Z = 1, 2$, and 3 for Xe^+, Xe^{2+}, and Xe^{3+} respectively, e is electron charge, m_i is ion mass. For $V_d = 200$ V, the ion bulk velocities $U_x^+ \approx 1.7 \times 10^4$ m/s, $U_x^{2+} \approx 2.4 \times 10^4$ m/s, and $U_x^{3+} \approx 2.96 \times 10^4$ m/s. The maximum velocity attained by the ions is limited by the applied voltage in the absence of any axial oscillations. However, some ions gain energy from the particle-wave interaction and have energy exceeding the limit imposed by the applied voltage.

Figure 5 shows IVDFs in x-v_x plane in the presence of 20% Xe^{2+} and 10% Xe^{3+}. Ion VDFs for the x-component of the velocity (v_x) is shown in Figs. 5(a), (b), and (c) for Xe^+, Xe^{2+}, and Xe^{3+}, respectively. The particles are binned into a discretized phase space with $\Delta x = 50\ \mu m$ and $\Delta v = 100$ m/s. In addition, Fig. 5(d) shows the IVDFs in the downstream, averaged from $x = 2$ cm to $x = 2.3$ cm.

Despite the presence of triply charged ions, the linear dispersion relation suggests that the growth rate and real frequency are not significantly modified. This is primarily because the doubly charged ion density is larger than triply charged ion density and therefore the resonant condition is mostly dictated by the interaction between singly and doubly charged ion streams. Similar to the observations in Ref. 32, the phase velocity, v_ϕ, of axial plasma wave can be estimated as $v_\phi = \omega/k_x \approx U_x^+ + c_s$, where ω and k are angular frequency and wave number of the plasma wave and c_s is ion acoustic speed. Figures 5(a)-(c) show the trapping of charged species around the phase velocity, $v_\phi \approx 2.15 \times 10^4$ m/s. As $U_x^+ \approx 1.7 \times 10^4$ m/s, this means that $c_s \approx 4.5 \times 10^3$ m/s, which is consistent with the ion acoustic speed evaluated using 30 eV electron temperature observed around $x \approx 1$ cm, where IITSI starts to grow[32]. The plasma wave results in Xe^+ ions that are higher energy than U_x^+ and a significant portion of Xe^{2+} to be decelerated, which are similarly observed in Ref. 32. The most notable result in the present study is that the trapping of Xe^{3+} can be seen from Fig. 5(d). It is interesting to note that the axial plasma wave results in (i) Xe^{3+} particles that are trapped around the phase velocity, forming a plateau

ACCEPTED MANUSCRIPT
Journal of Applied Physics
AIP Publishing
This is the author's peer reviewed, accepted manuscript. However, the online version of record will be different from this version once it has been copyedited and typeset.
PLEASE CITE THIS ARTICLE AS DOI: 10.1063/5.0067305

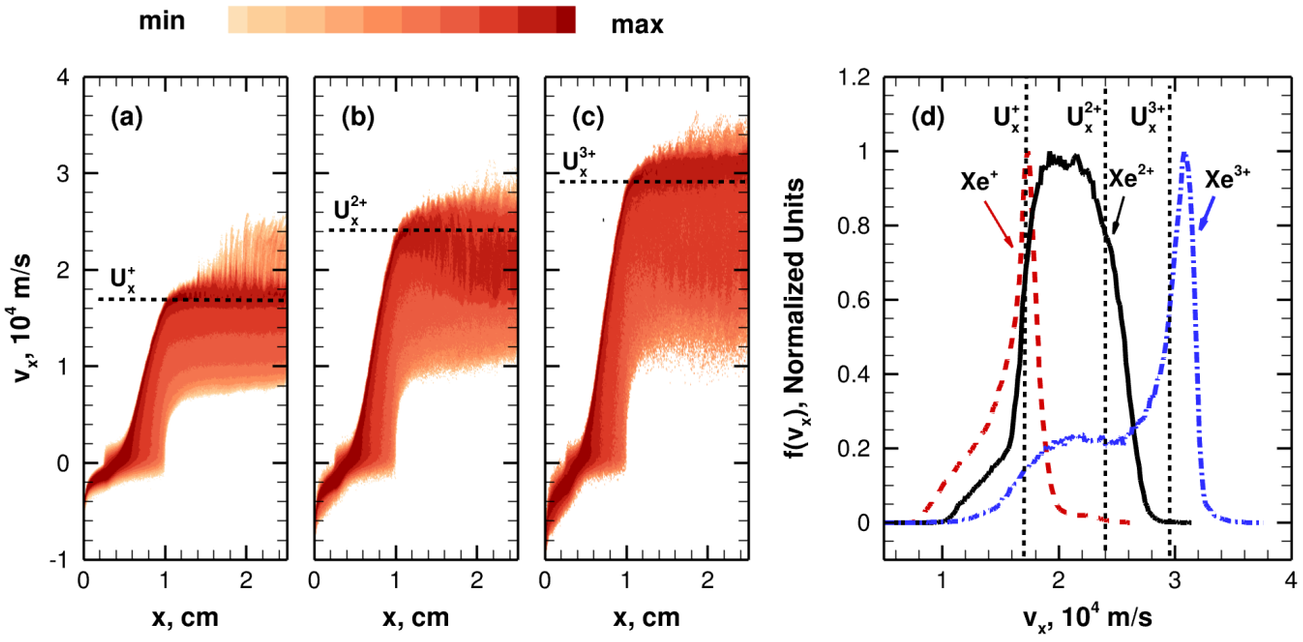

FIG. 5: Instantaneous ion velocity distribution function (IVDF) for the x-component (axial) of the velocity, averaged in the y direction is shown for (a) Xe^+ (b) Xe^{2+}, and (c) Xe^{3+}. The horizontal dashed lines indicate the ion bulk velocities assuming that the ions are accelerated across a constant voltage drop of 200 V. The colormap shows the VDFs normalized with the reference VDF values, which is chosen as $f^+_{\max}$ for Xe^+, $0.1 f^+_{\max}$ for Xe^{2+}, and $0.01 f^+_{\max}$ for Xe^{3+} where $f^+_{\max}$ is the maximum value of Xe^+ VDF. Colorbar uses logarithmic scale, where min and max correspond to 1.0 and 1.0×10^{-4} respectively. Shown in (d) are the axial VDFs in the plume ($2.0 \le x \le 2.3$ cm) for the three species.

in the Xe^{3+} IVDF, and (ii) Xe^{3+} particles with higher velocities than U_x^{3+}, i.e., the ballistic velocity predicted in Eq. (2), shifting the peak of the IVDF to a higher velocity.

To quantitatively estimate the efficiency of the ion acceleration, one can calculate the bulk velocity of the ions evaluated from the first moment of the IVDFs, i.e., $u = \int_0^\infty v\hat{f}(v)dv$, where v is the particle velocity and $\hat{f}$ is the normalized VDF. The bulk velocities of Xe^+, Xe^{2+}, and Xe^{3+} can be obtained from the IVDFs, shown in Fig. 5(d), as $u_x^+ = 1.61 \times 10^4$ m/s, $u_x^{2+} = 2.06 \times 10^4$ m/s, and $u_x^{3+} = 2.62 \times 10^4$ m/s, respectively. Using the ballistic velocities as shown in Eq. (2), if the beam acceleration efficiency is defined to be $\eta_b = (u_x/U_x)^2$, one obtains $\eta_b = 0.94$, 0.86, and 0.88, for Xe^+, Xe^{2+}, and Xe^{3+}, respectively. The lower beam acceleration efficiencies for Xe^{2+} and Xe^{3+} ions are consistent with the axial deceleration and collisionless thermalization due to the plasma wave, as shown in Fig. 1.

2. *Azimuthal IVDF*

Figure 6 shows the IVDFs in y-v_y plane of the three ion species considered in the simulation at two axial locations. The left column, Fig. 6(a), corresponds to the particles in the source region, i.e., $0.5 \le x \le 1$ cm, and the right column, Fig. 6(b), corresponds to the particles in the plume region, i.e., $1.4 \le x \le 2.5$ cm. The condition for nonlinear particle trapping within a sinusoidal potential wave can be written as,

$$|v_\phi - v_x^{Z+}| \ge \Delta v = \left(\frac{2Ze\phi_0}{m_i}\right)^{1/2}, \tag{3}$$

where v_x^{Z+} is the particle velocity for the different charge state $Z = 1, 2$, and 3, and ϕ_0 is the amplitude of the plasma wave. Thus, Eq. (3) shows that the higher charge states are more likely to be trapped within the potential waves.

Figure 6(a) shows that most ions are not fully trapped by the azimuthal plasma wave (E_y) within the source region. The trapping frequency[37] is given by

$$\omega_b = k\sqrt{\frac{2Ze\phi_0}{m_i}} = \sqrt{k\frac{2ZeE_0}{m_i}}, \tag{4}$$

where k is the wavenumber and $E_0 = \phi_0/k$ is the amplitude of the electric field fluctuation assuming a sinusoidal potential wave. From Fig. 1, $E_0 \approx 2 \times 10^4$ V/m and $k = 2\pi/\lambda_y = 9.55 \times 10^3$ rad/m in the source region, where λ_y is the wavelength of the plasma wave. This yields $\omega_b \approx 1.7 \times 10^7$ rad/s. Hence, the characteristic time for azimuthal particle trapping, $\tau_b = 2\pi/\omega_b$ is on the order of $0.4 - 1$ μs. On the other hand, the characteristic time for ion transit, $\tau_t = L/v_i$, is on the order of 0.1 μs. Hence, as $\tau_t < \tau_b$, there is not sufficient time to be fully trapped within the source region. It is to be noted that the Xe^{3+} show the formation of high velocity components,

ACCEPTED MANUSCRIPT
This is the author's peer reviewed, accepted manuscript. However, the online version of record will be different from this version once it has been copyedited and typeset.
PLEASE CITE THIS ARTICLE AS DOI: 10.1063/5.0067305
Journal of Applied Physics
AIP Publishing

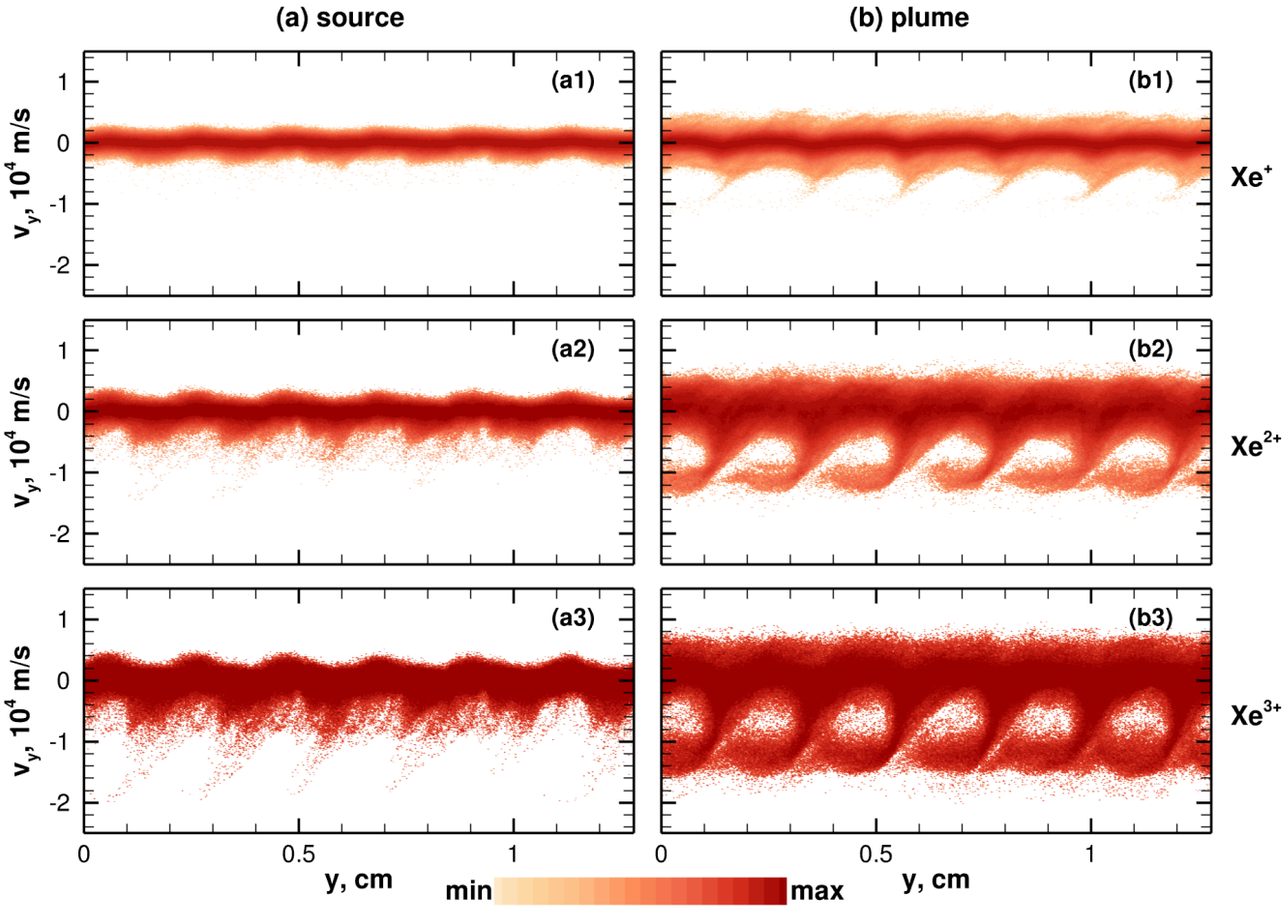

FIG. 6: Instantaneous ion velocity distribution function (IVDF) for the y-component (azimuthal) of the velocity, averaged in the x direction is shown for Xe^{+} in the top row, Xe^{2+} in the middle row, and Xe^{3+} in the bottom row. Two regions in the axial domain corresponding to (a) source ($0.5 \leq x \leq 1$ cm) and (b) plume ($1.4 \leq x \leq 2.5$ cm) are shown. Colormap is identical to Fig. 5.

which can be seen in Fig. 6(a3), because of the fastest trapping frequency ($Z = 3$), as shown in Eq. (3). However, such triply charged ions are not fully trapped either in the source region.

Figure 6(b) shows the azimuthal IVDFs in the plume region. The most interesting result is that the ion trapping feature is not observable for Xe^{+}, as shown in Fig. 6(b1), while Xe^{2+} and Xe^{3+} are fully trapped within the plasma waves, as shown in Figs. 6(b2) and (b3), respectively. It is to be noted that this feature is consistently found in other conditions despite the amount of the Xe^{3+} ions. It can be seen from Figs. 6(b2) and (b3) that the phase velocity of the azimuthal plasma wave is $v_\phi \approx 6 \times 10^3$ m/s, which is consistent with the ion acoustic speed evaluated using the electron temperature of 50 eV observed in $x \in [0.5\text{ cm}, 1\text{ cm}]$. Assuming a potential fluctuation amplitude of 10 V and using Eq. (3), the particles that are trapped within the potential wells must have a trapping velocity of $\Delta v = 3.5 \times 10^3$ m/s, 5.4×10^3 m/s, and 6.6×10^3 m/s for Xe^{+}, Xe^{2+}, and Xe^{3+}, respectively. It can therefore be concluded that $v_\phi > \Delta v$ for singly charged ions, leading to virtually no ion trapping. On the other hand, doubly and triply charged ions are trapped in the azimuthal direction as $v_\phi \leq \Delta v$ is satisfied.

The azimuthal IVDFs for the cross-field plasma in the presence of multiply charged ions are notably different from previous kinetic simulations where only singly charged ions are considered[27,38] because the only *trappable* ions are singly charged ions if multiply charged ions are not present in the simulation. The present results indicate that the IVDF measurements of Xe^{+}, e.g., using laser induced fluorescence, may not be able to detect such ion trapping phenomena. Based on the present kinetic simulations, Xe^{2+} and Xe^{3+} are more likely to exhibit such non-Maxwellian behavior. However, it is also to be noted that the ionization mechanism is simplified and is not self-consistently modeled in the present kinetic simulations. Thus, the degree of ion trapping may change depending on the location of the ion production within the discharge plasma. Additionally, as the present results show that the amplitude of the multidimensional plasma waves affects the electron transport, three-dimensional kinetic simulations are required to understand the electron transport in real sys-

ACCEPTED MANUSCRIPT
Journal of Applied Physics
AIP Publishing
This is the author's peer reviewed, accepted manuscript. However, the online version of record will be different from this version once it has been copyedited and typeset.
PLEASE CITE THIS ARTICLE AS DOI: 10.1063/5.0067305

tems.

IV. CONCLUSIONS

It was shown in Ref. 32 that singly and doubly charged ion streams excite the IITSI, which, through its nonlinear interaction with the ECDI, increases electron transport in the cross-field direction. In the present work, microturbulence developed due to these interactions between the ECDI and IITSI is now investigated accounting for a third (triply ionized) ion population, using a multidimensional kinetic simulation. Simulations were performed for several fractions of triply charged xenon ions while fixing the fraction of Xe^{2+} and other plasma characteristics, which sets up the ECDI and a large-amplitude IITSI.

The simulation results show that the IITSI driven by the relative velocities between singly, doubly, and triply charged xenon ions interacts nonlinearly with the ECDI. The mode coupling between ECDI and IITSI is shown to decrease the amplitudes of both axial and azimuthal plasma waves as the fraction of triply charged ions is increased. The 2D dispersion relation accounting for singly, doubly, and triply charged ion species and magnetized electrons, predicts a negligible effect of adding $\leq 10\%$ Xe^{3+} on the linear growth rate. However, the nonlinear saturation of different instabilities plays an important role in how large the amplitudes of plasma waves become. In particular, these results indicate approximately 30% damping in azimuthal amplitude (in the direction of $\mathbf{E}\times\mathbf{B}$ drift) and nearly 8% in axial amplitude (in the direction of applied $\mathbf{E}$ field and across the $\mathbf{B}$ field) when 10% triply charged xenon ions are added to the simulation. With an incremental increase in the fraction of triply charged ions from 0 to 10%, the cross-field electron transport is shown to reduce accordingly.

Ion species streaming with different velocities interact nonlinearly with the plasma wave and undergo trapping and heavily influence the saturation of these instabilities. Trapping of the three ion species near the source and in the plume shows that when amplitude of plasma wave driven by the IITSI is large enough, resonant particle-wave interactions take place and higher charge state ions are deeply trapped. This leads to broadening of the axial ion VDFs of all three species considered, where the Xe^{3+} VDF is shown to undergo the largest broadening due to the separation between the particle velocity and the phase velocity of the axial wave. In addition, the present simulations indicate that the singly charged ions may not be fully trapped within the azimuthal plasma wave driven by the ECDI. The multiply charged ions are more trapped because the trapping velocity scales as the charge state Z, which may play an important role in experimentally detecting such ion trapping features. The results of this paper are relevant to partially magnetized devices in which a diversity of ion charge states are generated. These findings show the extent to which the presence of multiple charge states influences the nonlinear behavior of key instabilities and their contribution to anomalous transport.

ACKNOWLEDGMENTS

This material is based on work supported by the Air Force Office of Scientific Research under Award No. FA9550-18-1-0090 and by the US Department of Energy, Office of Science, Office of Fusion Energy Sciences, under Award No. DE-SC0020623. Simulations are performed using the high performance computing resources at the Stanford Research Computing Center.

DATA AVAILABILITY STATEMENT

The data that support the findings of this study are available from the corresponding author upon reasonable request.

[1] E. Doyle *et al.*, "Chapter 2: Plasma confinement and transport," Nuclear Fusion **47**, S18–S127 (2007).
[2] J.-P. Boeuf, "Tutorial: Physics and modeling of Hall thrusters," Journal of Applied Physics **121**, 011101 (2017).
[3] A. Morozov, "The conceptual development of stationary plasma thrusters," Plasma Physics Reports **29**, 235–250 (2003).
[4] J.-P. Boeuf and B. Chaudhury, "Rotating instability in low-temperature magnetized plasmas," Physical Review Letters **111**, 155005 (2013).
[5] J. Cavalier, N. Lemoine, G. Bonhomme, S. Tsikata, C. Honoré, and D. Grésillon, "Hall thruster plasma fluctuations identified as the $\mathbf{E}\times\mathbf{B}$ electron drift instability: Modeling and fitting on experimental data," Physics of Plasmas **20**, 082107 (2013).
[6] A. I. Smolyakov, O. Chapurin, W. Frias, O. Koshkarov, I. Romadanov, T. Tang, M. Umansky, Y. Raitses, I. D. Kaganovich, and V. P. Lakhin, "Fluid theory and simulations of instabilities, turbulent transport and coherent structures in partially-magnetized plasmas of $\mathbf{E}\times\mathbf{B}$ discharges," Plasma Physics and Controlled Fusion **59**, 014041 (2016).
[7] A. W. Smith and M. A. Cappelli, "Time and space-correlated plasma potential measurements in the near field of a coaxial Hall plasma discharge," Physics of Plasmas **16**, 073504 (2009).
[8] S. Yoshikawa and D. Rose, "Anomalous diffusion of a plasma across a magnetic field," The Physics of Fluids **5**, 334–340 (1962).
[9] J. Parker, Y. Raitses, and N. Fisch, "Transition in electron transport in a cylindrical Hall thruster," Applied Physics Letters **97**, 091501 (2010).
[10] C. Ellison, Y. Raitses, and N. J. Fisch, "Cross-field electron transport induced by a rotating spoke in a cylindrical Hall thruster," Physics of Plasmas **19**, 013503 (2012).
[11] I. G. Mikellides and I. Katz, "Numerical simulations of Hall-effect plasma accelerators on a magnetic-field-aligned mesh," Physical Review E **86**, 046703 (2012).
[12] K. Hara, "An overview of discharge plasma modeling for Hall effect thrusters," Plasma Sources Science and Technology **28**, 044001 (2019).
[13] T. Charoy, J.-P. Boeuf, A. Bourdon, J. A. Carlsson, P. Chabert, B. Cuenot, D. Eremin, L. Garrigues, K. Hara, I. D. Kaganovich, *et al.*, "2D axial-azimuthal particle-in-cell benchmark for low-temperature partially magnetized plasmas," Plasma Sources Science and Technology **28**, 105010 (2019).
[14] J.-P. Boeuf and L. Garrigues, "$\mathbf{E}\times\mathbf{B}$ electron drift instability in Hall thrusters: Particle-in-cell simulations vs. theory," Physics of Plasmas **25**, 061204 (2018).
[15] S. Barral and E. Ahedo, "Low-frequency model of breathing oscillations in Hall discharges," Physical Review E **79**, 046401 (2009).
[16] M. Keidar, I. Boyd, and I. Beilis, "Plasma flow and plasma–wall transition in Hall thruster channel," Physics of Plasmas **8**, 5315–5322 (2001).
[17] J. Adam, A. Héron, and G. Laval, "Study of stationary plasma thrusters using two-dimensional fully kinetic simulations," Physics of Plasmas **11**, 295–305 (2004).
[18] A. Héron and J. Adam, "Anomalous conductivity in Hall thrusters: Effects of the non-linear coupling of the electron-cyclotron drift instability with secondary electron emission of the walls," Physics of Plasmas **20**, 082313 (2013).

ACCEPTED MANUSCRIPT
Journal of Applied Physics
AIP Publishing
This is the author's peer reviewed, accepted manuscript. However, the online version of record will be different from this version once it has been copyedited and typeset.
PLEASE CITE THIS ARTICLE AS DOI: 10.1063/5.0067305

[19]W. Yan, F. Liu, C. Sang, and D. Wang, "Two-dimensional modeling of the cathode sheath formation during the streamer-cathode interaction," Physics of Plasmas **21**, 013504 (2014).
[20]S. Cho, K. Komurasaki, and Y. Arakawa, "Kinetic particle simulation of discharge and wall erosion of a Hall thruster," Physics of Plasmas **20**, 063501 (2013).
[21]J. M. Fife, *Hybrid-PIC modeling and electrostatic probe survey of Hall thrusters*, Ph.D. thesis, Massachusetts Institute of Technology (1998).
[22]J. Bareilles, G. Hagelaar, L. Garrigues, C. Boniface, J. Boeuf, and N. Gascon, "Critical assessment of a two-dimensional hybrid Hall thruster model: Comparisons with experiments," Physics of Plasmas **11**, 3035–3046 (2004).
[23]F. I. Parra, E. Ahedo, J. M. Fife, and M. Martínez-Sánchez, "A two-dimensional hybrid model of the Hall thruster discharge," Journal of Applied Physics **100**, 023304 (2006).
[24]L. Muschietti and B. Lembège, "Microturbulence in the electron cyclotron frequency range at perpendicular supercritical shocks," Journal of Geophysical Research: Space Physics **118**, 2267–2285 (2013).
[25]S. Tsikata, J. Cavalier, A. Héron, C. Honoré, N. Lemoine, D. Grésillon, and D. Coulette, "An axially propagating two-stream instability in the Hall thruster plasma," Physics of Plasmas **21**, 072116 (2014).
[26]W. Villafana, F. Petronio, A. C. Denig, M. J. Jimenez, D. Eremin, L. Garrigues, F. Taccogna, A. Alvarez-Laguna, J. P. Boeuf, A. Bourdon, P. Chabert, T. Charoy, B. Cuenot, K. Hara, F. Pechereau, A. Smolyakov, D. Sydorenko, A. Tavant, and O. Vermorel, "2D radial-azimuthal particle-in-cell benchmark for $\mathbf{E}\times\mathbf{B}$ discharges," Plasma Sources Science and Technology **30**, 075002 (2021).
[27]T. Lafleur, S. Baalrud, and P. Chabert, "Theory for the anomalous electron transport in Hall effect thrusters. ii. kinetic model," Physics of Plasmas **23**, 053503 (2016).
[28]F. S. Gulczinski III and A. D. Gallimore, "Near-field ion energy and species measurements of a 5-kw Hall thruster," Journal of Propulsion and Power **17**, 418–427 (2001).
[29]J. Bohlmark, M. Lattemann, J. Gudmundsson, A. Ehiasarian, Y. A. Gonzalvo, N. Brenning, and U. Helmersson, "The ion energy distributions and ion flux composition from a high power impulse magnetron sputtering discharge," Thin Solid Films **515**, 1522–1526 (2006).
[30]S. D. Baalrud, C. C. Hegna, and J. D. Callen, "Instability-enhanced collisional friction can determine the bohm criterion in multiple-ion-species plasmas," Phys. Rev. Lett. **103**, 205002 (2009).
[31]W. Kasparek and E. Holzhauer, "Co2-laser scattering from thermal fluctuations in a plasma with two ion components," Physical Review A **27**, 1737 (1983).
[32]K. Hara and S. Tsikata, "Cross-field electron diffusion due to the coupling of drift-driven microinstabilities," Physical Review E **102**, 023202 (2020).
[33]H. Du, Z.-X. Wang, and J. Dong, "Impurity effects on trapped electron mode in tokamak plasmas," Physics of Plasmas **23**, 072106 (2016).
[34]M. A. Lieberman and A. J. Lichtenberg, *Principles of Plasma Discharges and Materials Processing, Second Edition* (John Wiley & Sons, Inc., 2005).
[35]K. Hara, I. D. Boyd, and V. I. Kolobov, "One-dimensional hybrid-direct kinetic simulation of the discharge plasma in a Hall thruster," Physics of Plasmas **19**, 113508 (2012).
[36]K. Hara, M. J. Sekerak, I. D. Boyd, and A. D. Gallimore, "Mode transition of a Hall thruster discharge plasma," Journal of Applied Physics **115**, 203304 (2014).
[37]K. Hara, T. Chapman, J. W. Banks, S. Brunner, I. Joseph, R. L. Berger, and I. D. Boyd, "Quantitative study of the trapped particle bunching instability in langmuir waves," Physics of Plasmas **22**, 022104 (2015).
[38]T. Lafleur, S. D. Baalrud, and P. Chabert, "Theory for the anomalous electron transport in Hall effect thrusters. i. insights from particle-in-cell simulations," Physics of Plasmas **23**, 053502 (2016).
[39]C. Honoré, D. Grésillon, S. Tsikata, J. Cavalier, D. Coulette, N. Lemoine, G. Largeau, and G. Daniel, "Micro fluctuation control and Hall thruster operation," 40th European Physical Society Conference on Plasma Physics, Espoo, Finland **P5.407** (2013).
[40]E. Choueiri, "Plasma oscillations in Hall thrusters," Physics of Plasmas **8**, 1411–1426 (2001).
[41]P. Coche and L. Garrigues, "A two-dimensional (azimuthal-axial) particle-in-cell model of a Hall thruster," Physics of Plasmas **21**, 023503 (2014).

ACCEPTED MANUSCRIPT
Journal of Applied Physics
AIP Publishing
This is the author's peer reviewed, accepted manuscript. However, the online version of record will be different from this version once it has been copyedited and typeset.
PLEASE CITE THIS ARTICLE AS DOI: 10.1063/5.0067305

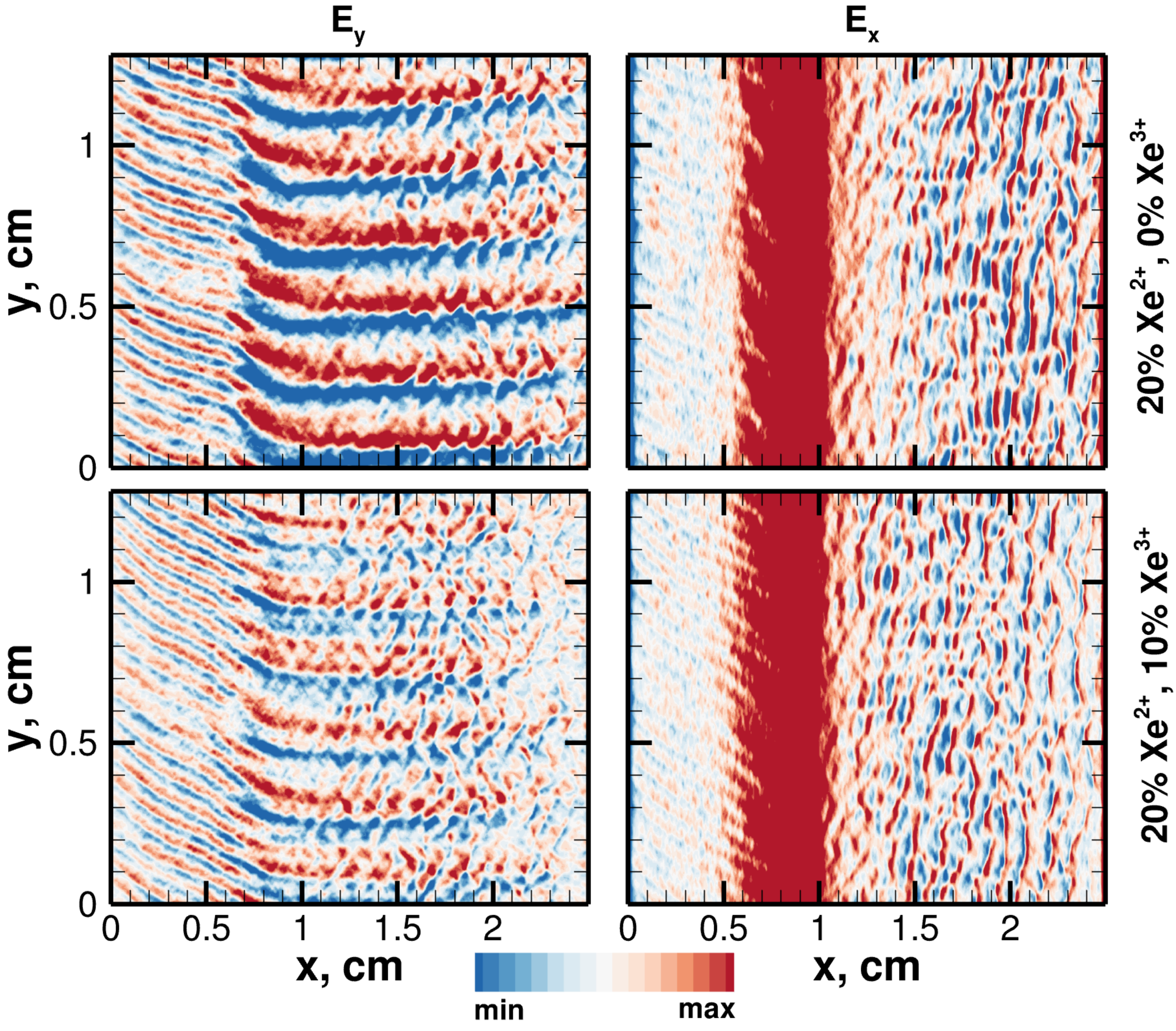

ACCEPTED MANUSCRIPT
Journal of Applied Physics
AIP Publishing
This is the author's peer reviewed, accepted manuscript. However, the online version of record will be different from this version once it has been copyedited and typeset.
PLEASE CITE THIS ARTICLE AS DOI: 10.1063/5.0067305

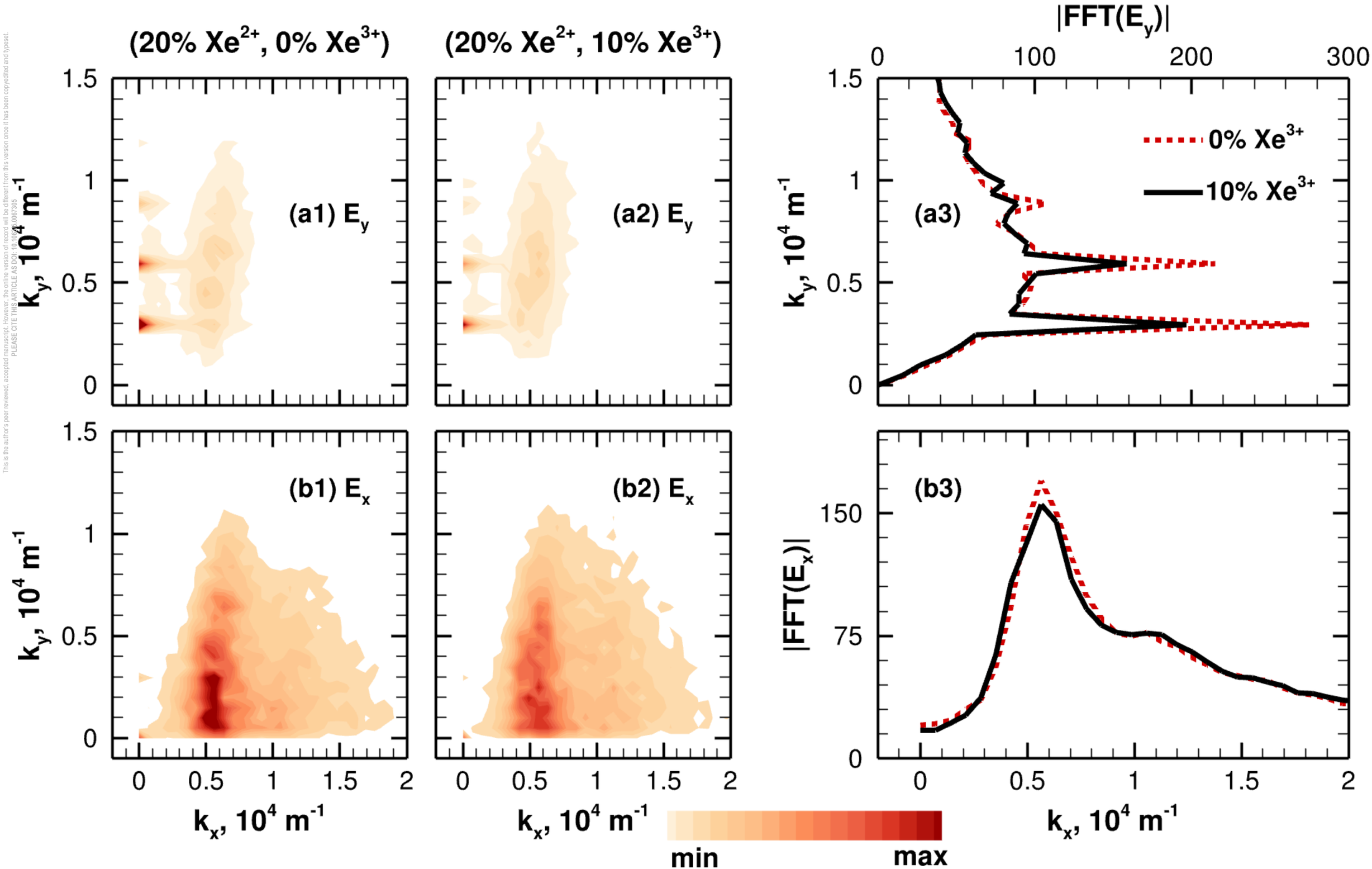

ACCEPTED MANUSCRIPT
Journal of Applied Physics
AIP Publishing
This is the author's peer reviewed, accepted manuscript. However, the online version of record will be different from this version once it has been copyedited and typeset.
PLEASE CITE THIS ARTICLE AS DOI: 10.1063/5.0000765

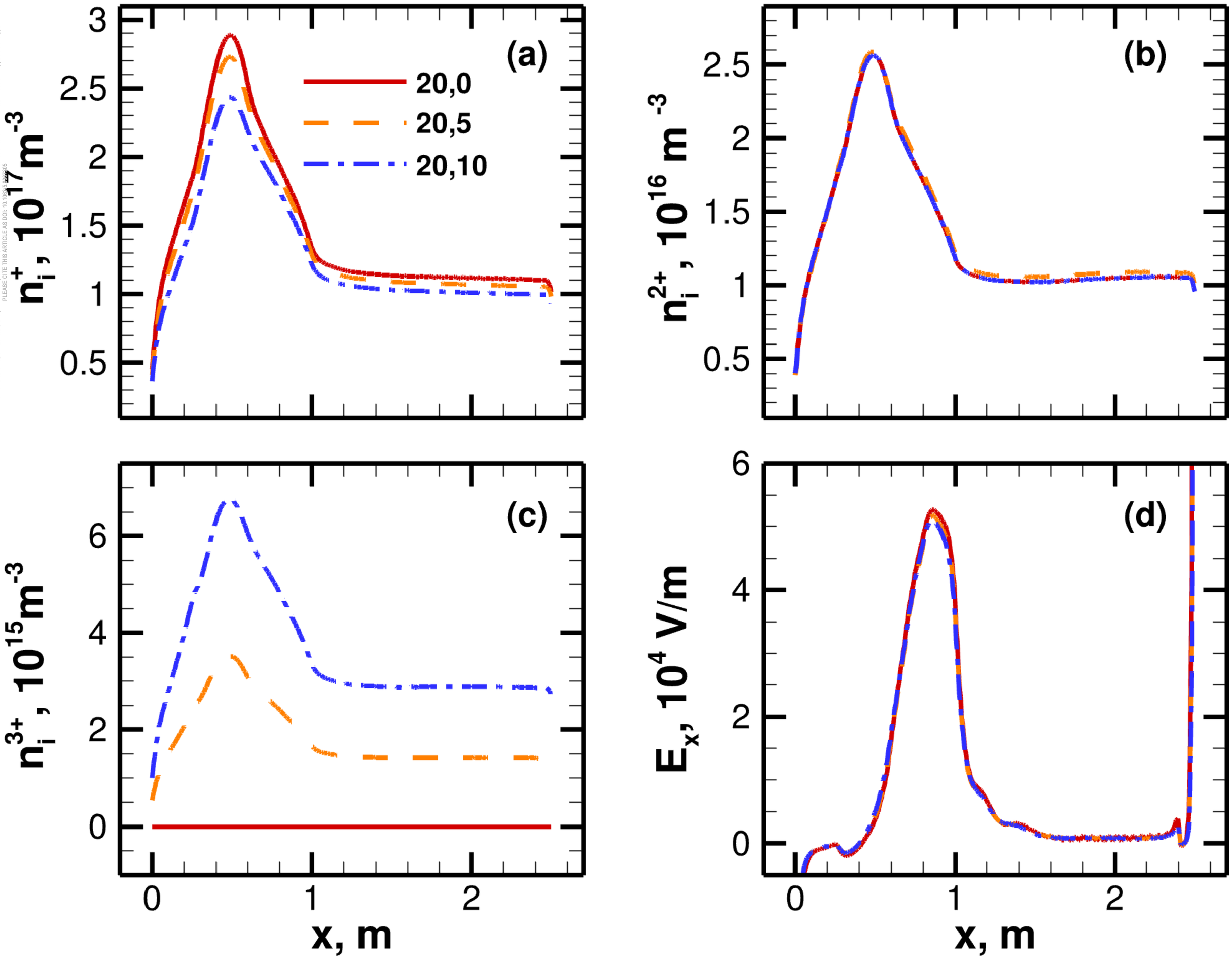

ACCEPTED MANUSCRIPT
Journal of Applied Physics
AIP Publishing
This is the author's peer reviewed, accepted manuscript. However, the online version of record will be different from this version once it has been copyedited and typeset.
PLEASE CITE THIS ARTICLE AS DOI: 10.1063/5.0067305

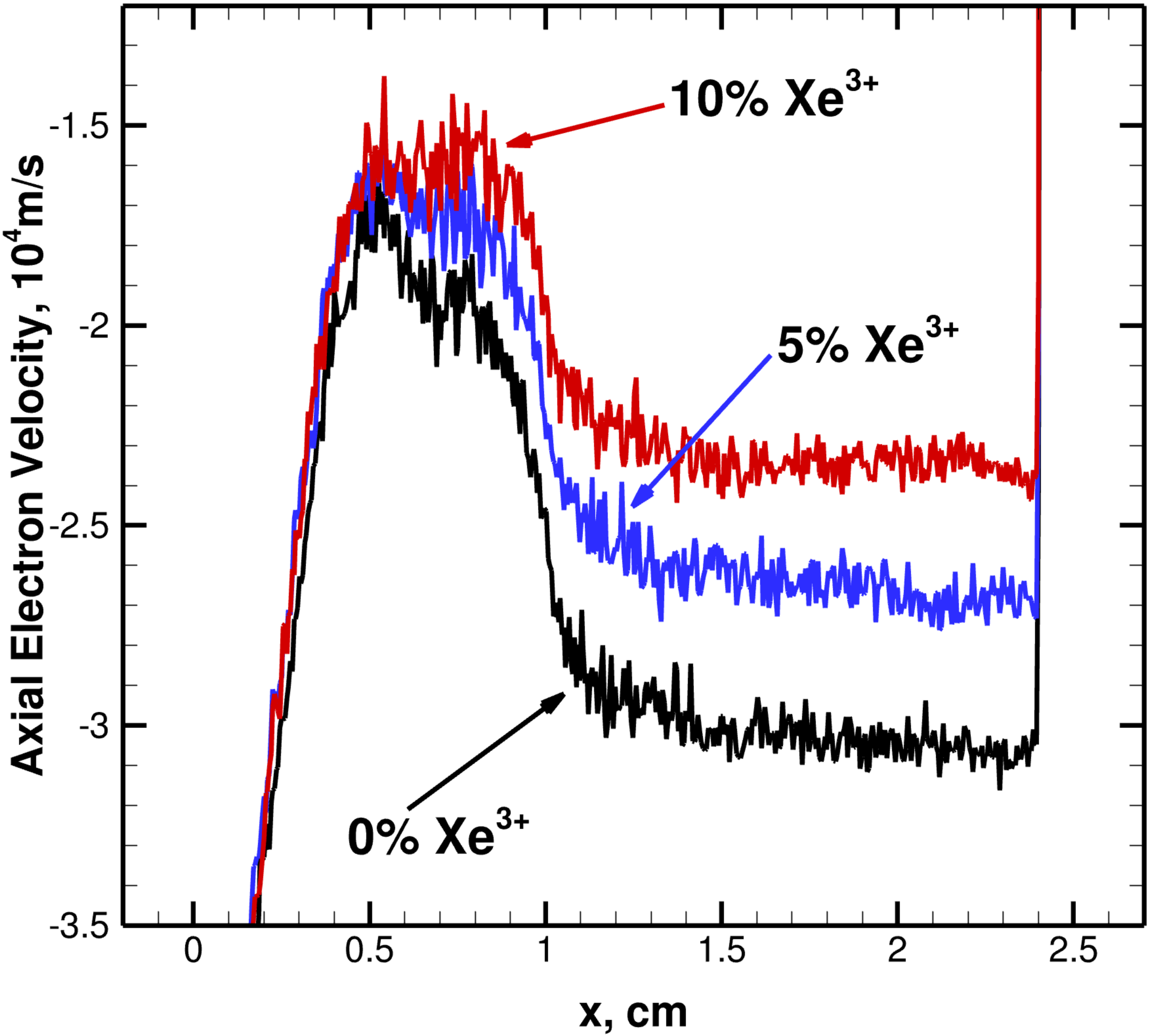

ACCEPTED MANUSCRIPT
Journal of Applied Physics
AIP Publishing
This is the author's peer reviewed, accepted manuscript. However, the online version of record will be different from this version once it has been copyedited and typeset.
PLEASE CITE THIS ARTICLE AS DOI: 10.1063/5.0067305

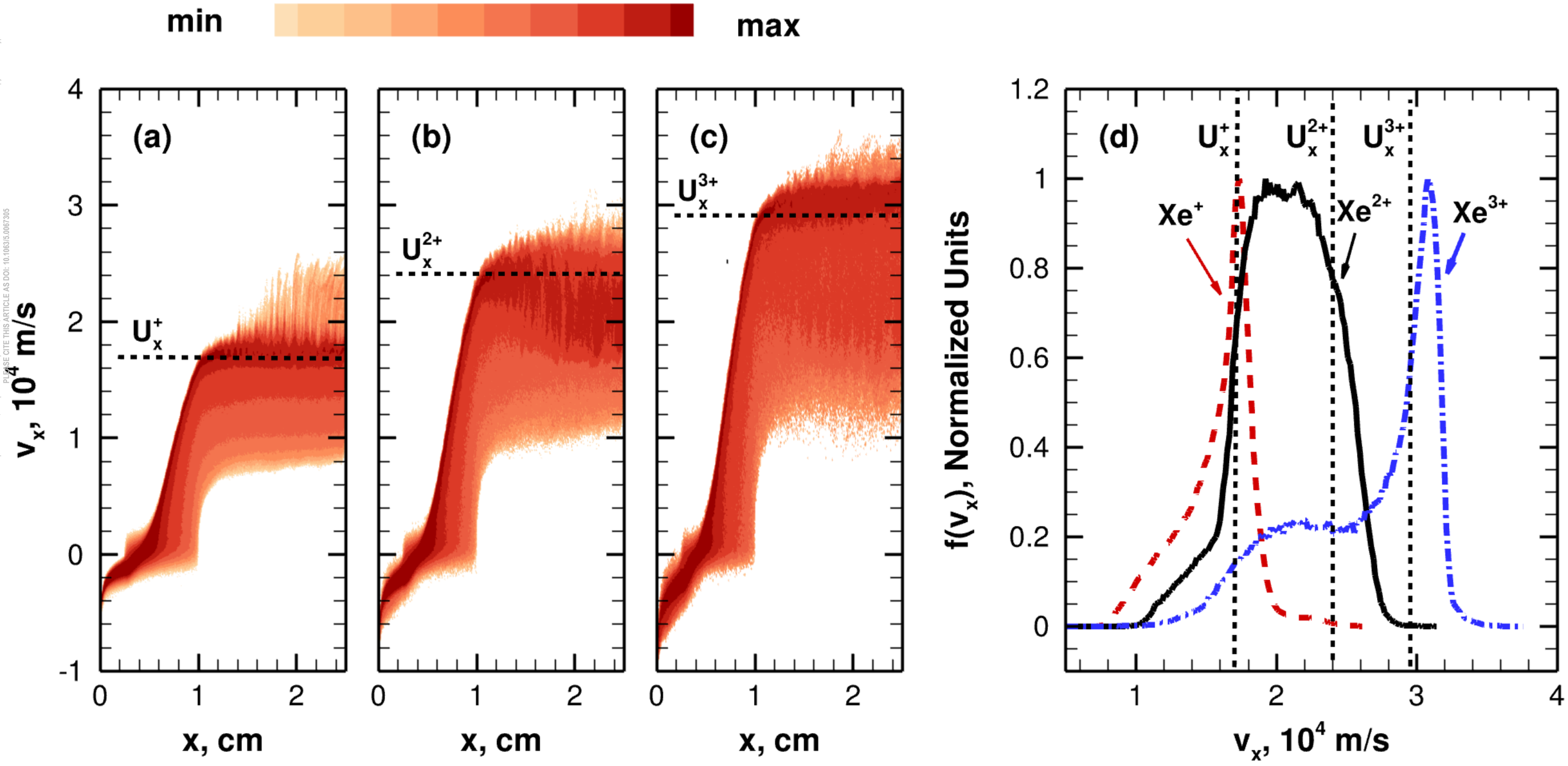
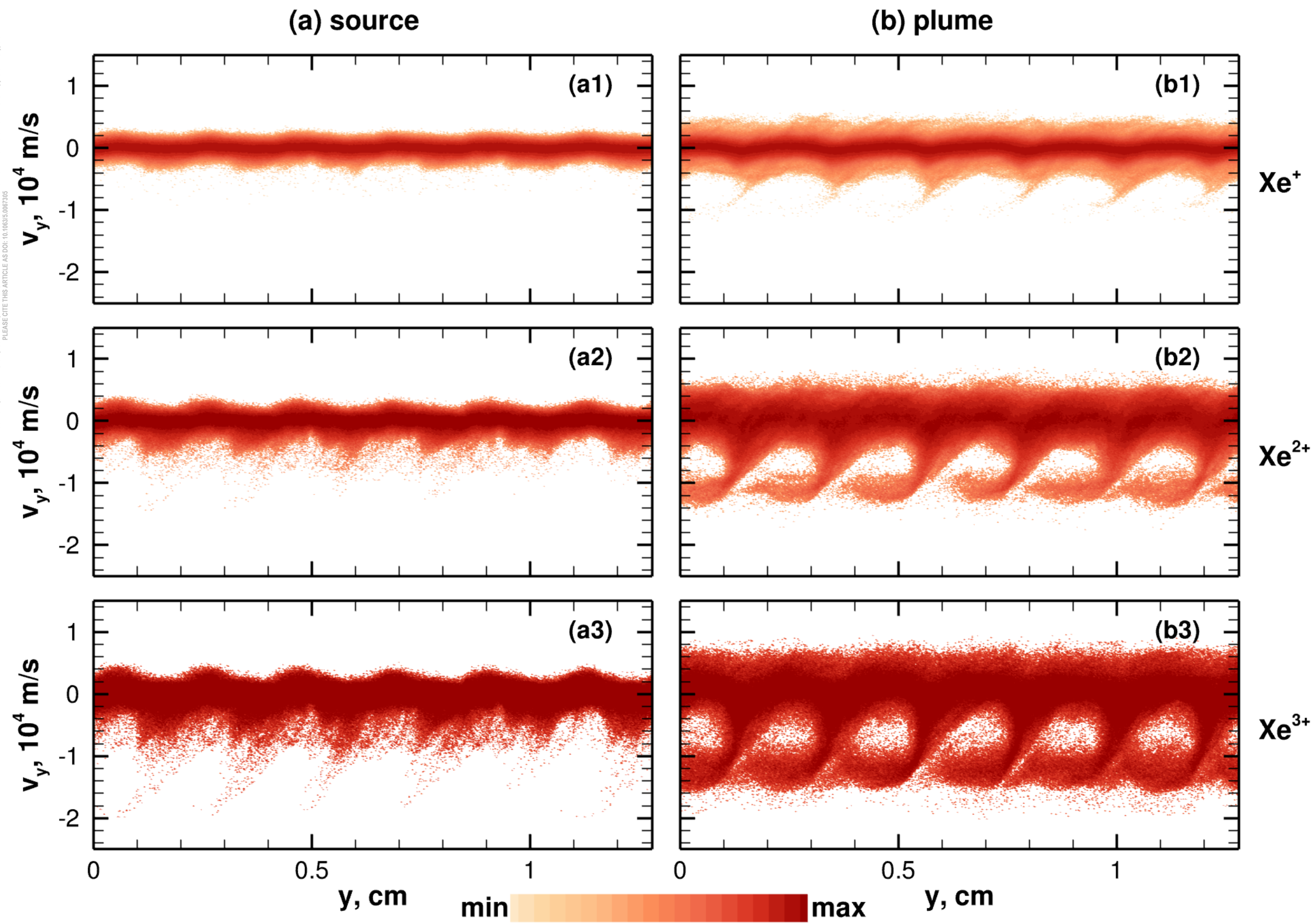
ACCEPTED MANUSCRIPT
Journal of Applied Physics
AIP Publishing
This is the author's peer reviewed, accepted manuscript. However, the online version of record will be different from this version once it has been copyedited and typeset.
PLEASE CITE THIS ARTICLE AS DOI: 10.1063/5.0067305